

The SED in the hot continuum of the symbiotic binary AR Pavonis

I. Tests with current models

A. Skopal¹

*Astronomical Institute, Slovak Academy of Sciences, 059 60 Tatranská Lomnica,
Slovakia*

Abstract

We present the spectral energy distribution (SED) in the continuum of the eclipsing symbiotic binary AR Pav between 0.12 and 3.4 μm . This revealed a high luminosity of the hot object in the binary, $L_h \sim 2200 (d/4.9 \text{ kpc})^2 L_\odot$. We introduce a method of disentangling the total continuum spectrum into its individual components of radiation for current models of symbiotic binaries. Applying a standard ionization model we show that the configuration of AR Pav differs significantly from that typical for symbiotic binaries during their quiescent phases. The best fit of the observed SED is provided by radiation of a simple blackbody accretion disk with $L_{\text{AD}} \sim 1700 (d/4.9 \text{ kpc})^2 L_\odot$, which is embedded in an extended hot corona with $T_e = 40\,000 \pm 5\,000 \text{ K}$ and $L_N \sim 500 (d/4.9 \text{ kpc})^2 L_\odot$. This basic configuration of the hot object explains also the observed wavelength-dependent depth and width of the eclipse profile. The standard thin disk model requires a high accretion rate $\dot{M}_{\text{acc}} \gtrsim 2 \times 10^{-4} M_\odot \text{ yr}^{-1}$ onto the central star with a radius $R_{\text{acc}} \gtrsim 2 R_\odot$ to balance the observed luminosity. Even irrespectively to the disk model, the accretion process limits $R_{\text{acc}} > 0.1 R_\odot$ for $\dot{M}_{\text{acc}} > 1.7 \times 10^{-5} M_\odot \text{ yr}^{-1}$ and $M_{\text{acc}} = 0.75 - 1.0 M_\odot$, which precludes a white dwarf to be the accreting star. Application of models with the disk and the boundary layer shows that the far-UV spectrum is not consistent with a large amount of a hot radiation from the boundary layer. However, the presence of such a boundary layer in the system is indirectly indicated through the strong nebular emission. This solution suggests that the hotter inner parts of the disk including the boundary layer are occulted by the disk material in the direction to the observer.

Key words: Eclipsing binaries, Symbiotic stars, Accretion and accretion disks
PACS: 97.80.Hn, 97.80.Gm, 97.10.Gz

¹ E-mail: skopal@ta3.sk

1 Introduction

AR Pavonis was discovered by Mayall (1937) as an eclipsing P-Cygni type star with a period of 605 days. Andrews (1974) found that the eclipsed object is highly variable in both brightness and size. On the basis of ultraviolet spectroscopy Hutchings et al. (1983) confirmed this view. Bruch, Niehues and Jones (1994) observed a periodic ($\sim P_{\text{orb}}$) wave-like variation, which occurred in the visual light curve between eclipses from 1985.7. As the most satisfying explanation they suggested a brightness modulation due to variation in the mass transfer rate from the red giant to the hot component. Analysing historical 1889–1998 light curve, Skopal et al. (2000a) identified the real change of the orbital period at a rate $\dot{P} = -3.5 \pm 0.8 \times 10^{-5}$ between 1896 April and 1985 September. They also noted that during quiescence, the light curve has characteristic features similar to those observed in CVs. Recently, Skopal et al. (2001a) refined the mean orbital period to 604.45 ± 0.02 days.

As to the AR Pav configuration, Thackeray and Hutchings (1974) proposed a binary model, in which the red giant fills its Roche lobe and loses mass to an evolved, $\sim 30\,000$ K hot, compact object surrounded by a moderately dense gas cloud or a thick ring. Kenyon and Webbink (1984) found that the observed UV continuum colours for AR Pav are well comparable to those derived from a model of an accretion disk around a main sequence accretor. Recently, Schild et al. (2001), having new radial velocities of the red giant, determined its mass function to $0.055 M_{\odot}$ and the projected rotation velocity of $11 \pm 2 \text{ km s}^{-1}$. Assuming co-rotation, they derived the giant radius of $130 R_{\odot}$ and by comparing its adequate stellar parameters with RGB/AGB evolutionary tracks in the HR diagram, they suggested the giant mass as $2 M_{\odot}$, and, consequently from the mass function, the hot component mass as $0.75 M_{\odot}$. Based on these parameters, Schild et al. (2001) suggested that the hot component in AR Pav is most probably a white dwarf and the cool component is deeply inside of its Roche lobe (however, as we will show later in this paper, the giant in this system does most probably fill its Roche lobe). Most recently, Quiroga et al. (2002), having radial velocities of both components, determined their masses as $M_g = 2.5 M_{\odot}$, $M_h = 1 M_{\odot}$. They obtained the radial velocity curve of the hot star under assumption that the broad emission wings of the H α , H β and He II 4686 profiles originate from the inner accretion disk or an envelope around the central star. In addition, the authors suggested that the central absorption in hydrogen line profiles is formed in the neutral part of the giant's wind, which is concentrated in the orbital plane.

In this paper we analyse the SED in the continuum between 0.12 and $3.4 \mu\text{m}$ with the aim to determine a basic configuration of the hot object in AR Pav. In Sect. 3 we introduce individual components of radiation often used in interpretation of the spectra of symbiotic stars. In Sect. 4 we compare the observed

SED and those given by current models of symbiotic stars, including a standard ionization model and models with an accretion disk. Finally, in Sect. 5 we discuss their physical plausibility and suggest basic structure of the hot object.

2 Observations

To reconstruct the SED of AR Pav in the range of 0.12 to $3.4\,\mu\text{m}$ we used the broad-band optical and infrared *UBVRI* and *JHKL* photometry and the IUE (International Ultraviolet Explorer) low-resolution spectroscopy.

The optical/IR magnitudes were summarized by Skopal et al. (2000a) and some new observations were recently published by Skopal et al. (2000b). To determine the star's brightness in eclipses we used photometric measurements of Andrews (1974) and Menzies et al. (1982). Observations in the R_{C} and I_{C} bands of the Cousins system were transformed into the Johnson system according to Bessell (1983). Stellar magnitudes were converted to fluxes according to the calibration of Léna, Lebrun and Mignard (1999).

The ultraviolet fluxes were taken from Fig. 5 of Schild et al. (2001). We used average values from those measured out of eclipses (i.e. between orbital phases $0.91 > \varphi > 1.1$; the rms within 10-15%) and values from the mid eclipse. To get better coverage of the ultraviolet continuum we added a few values from Fig. 2 of Hutchings et al. (1983) and measurements presented in Table 4 of Kenyon and Webbink (1984).

Finally, we dereddened observations with $E_{\text{B-V}} = 0.26$ (Kenyon and Webbink, 1984) using the extinction curve of Mathis (1987) in the UV/optical region, while in the IR wavelengths we used reddening ratios of Savage and Mathis (1979). Table 1 summarizes the observations used in our paper.

3 Spectral energy distribution

Figure 1 shows the $0.12 - 3.4\,\mu\text{m}$ SED in the continuum of AR Pav. This suggests a high luminosity of the hot object, similar to that of its cool companion. The out-of-eclipse continuum is characterized by: (i) A round far-UV shape with decreasing fluxes to shorter wavelengths, and (ii) a flat profile in the near-UV/optical region. Both the steep far-UV ($\lambda < 1\,500\,\text{\AA}$) continuum and the prominent Balmer jump in emission – characteristic features of the continuum of symbiotic stars during quiescence – are not present. We will fit the out-of-eclipse continuum by that including an accretion disk, but also test

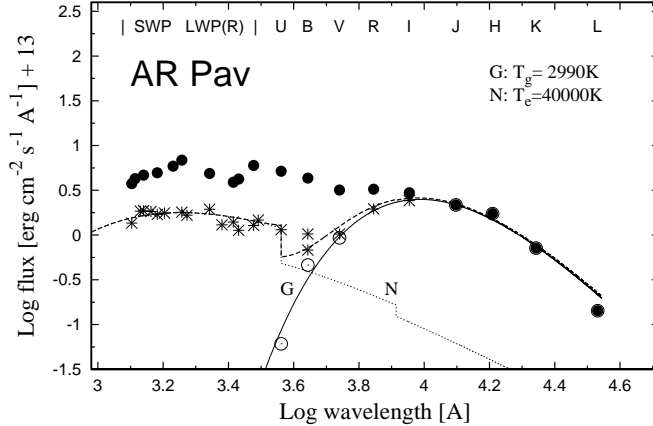


Fig. 1. Dereddened fluxes of the AR Pav continuum given by the low-resolution IUE spectra, optical *UBVRI* and infrared *JHKL* photometry (Table 1). Measurements made during eclipses are marked by (*), out of eclipses by (●), and open circles (○) correspond to fluxes of the giant derived from its spectral type (Menzies et al., 1982). Observations during eclipses can be approximated by nebular continuum of $T_e = 40\,000$ K (N) and fluxes of the giant by a Planck function of the colour temperature $T_g = 2\,990$ K (G). The dashed thick line represents their sum.

whether a standard ionization model of symbiotic binaries can explain these characteristics.

During eclipses, the ultraviolet continuum weakened by a factor of $\sim 3\text{--}5$, it is flatter than that observed out of eclipses and displays a discontinuity at *U/B*. This suggests the nebular-type spectrum of a very hot gas. We will fit the uneclipsed continuum by the nebular radiation of a high electron temperature. In the following sections we describe simple models of the considered components of radiation, which we use to fit the observed SED.

3.1 Nebular continuum

In the conditions of ionized gaseous nebulae in symbiotic stars (a dense medium with $n_e \sim 10^6 - 10^{11} \text{ cm}^{-3}$), the main contributor to the near-UV/optical continuum is the free-bound (f-b) emission from hydrogen. Less important are the f-b emission of He II and He I. Due to the dominance of the H I f-b emission and its basically similar profile with that of He I and He II (see Fig. 1 of Brown and Mathews, 1970), and also for the sake of simplicity, we calculate here only H I f-b and f-f nebular contributions. The nebular flux is proportional to $\int n_+ n_e dV$, where n_+ and n_e is the concentration of protons and electrons, respectively. Accordingly, the observed flux, F_λ^{obs} ($\text{erg cm}^{-2} \text{ s}^{-1} \text{ Å}^{-1}$), of the nebular continuum at the wavelength λ , can be written as

$$4\pi d^2 F_\lambda^{\text{obs}} = \varepsilon_\lambda \int_V n_+ n_e dV, \quad (1)$$

Table 1

Continuum fluxes between 0.12 and 3.4 μm .

$\lambda[\text{\AA}]$	F_{obs}	F_{der}	F_{obs}	F_{der}	Ref.
	in eclipses		out of eclipses		
1270	0.15	1.36	0.40	3.75	3
1300			0.48	4.27	4
1350	0.23	1.85			3
1380	0.25	1.87	0.64	4.67	5
1455	0.26	1.83			3
1520	0.25	1.70	0.73	4.96	5
1600	0.27	1.76			3
1700			0.91	5.88	4
1808	0.28	1.80	1.07	6.87	5
1875	0.26	1.67			3
2200	0.20	1.94	0.50	4.88	3,4
2400	0.23	1.30			3
2600	0.29	1.40	0.80	3.89	3,4
2700	0.25	1.13	0.93	4.22	5
3000	0.34	1.28	1.59	6.00	5
3100	0.40	1.47			3
3645	0.52	1.60	1.71	5.16	2
4400	0.41	1.03	1.66	4.33	2
4400	0.27	0.68			6
5500	0.49	1.03	1.52	3.19	2
7000	1.14	1.99	1.86	3.25	2
9000			1.86	2.66	2
12500			1.77	2.17	1
16200			1.50	1.74	1
22000			0.65	0.72	1
34000			0.14	0.14	1

Fluxes are in $10^{-13} \text{ erg cm}^{-2} \text{ s}^{-1} \text{ \AA}^{-1}$

Ref.: 1 - Glass and Webster (1973), 2 - Menzies et al. (1982), 3 - Hutchings et al. (1983), 4 - Kenyon and Webbink (1984), 5 - Schild et al. (2001), 6 - Andrews (1974)

in which d is the distance to the object, V is the volume of the ionized zone and ε_λ (erg cm³ s⁻¹ Å⁻¹) is the total (f-b + f-f) volume emission coefficient per electron and per ion in the wavelength scale. We calculated them according to expressions given by Brown and Mathews (1970) adopting the Gaunt factors to be unity. In spite of this approximation, our procedure reproduces the tabulated values (Brown and Mathews, 1970; Gurzadyan, 1997) within $\sim 5\%$ at the blue side of the Balmer discontinuity and within 1% or less at other wavelengths for electron temperatures $T_e \sim 10\,000 - 20\,000$ K. The difference is smaller for higher T_e .

3.2 Blackbody accretion disk and the boundary layer continuum

Because of having defined the continuum only by fluxes at selected wavelengths (i.e. only the continuous radiation can be investigated), we will assume a steady-state, time-independent accretion disk around a central star of mass M_{acc} and radius R_{acc} . Further, the accretion disk is optically thick and radiates locally like a blackbody (e.g. Tylenda, 1981). The source of its energy is the gravitational potential energy of the accretor. The observed flux distribution of the disk, F_λ , is then given by contributions of blackbody annuli integrated through the entire disk. The flux emitted by each annulus at the radial distance r is weighted by its area, $2\pi r dr$. Thus the observed flux distribution of a disk at a distance d can be written as

$$F_\lambda = \frac{2\pi \cos(i)}{d^2} \int_{R_{\text{acc}}}^{R_d} B_\lambda(T_{\text{eff}}(r)) r dr, \quad (2)$$

where i is the inclination of the disk, R_d its radius, and the radial temperature structure of the disk,

$$T_{\text{eff}}(r) = T_* \left[\frac{R_{\text{acc}}}{r} \right]^{3/4} \left\{ 1 - \left[\frac{R_{\text{acc}}}{r} \right]^{1/2} \right\}^{1/4}, \quad (3)$$

where

$$T_* = 4.10 \times 10^4 R_9^{-3/4}(\text{acc}) M_1^{1/4}(\text{acc}) \dot{M}_{16}^{1/4}(\text{acc}) \text{ K}, \quad (4)$$

in which R_9 and M_{acc} are the radius and mass of the accretor and \dot{M}_{16} is the accretion rate (Warner, 1995). The notation X_n means that the parameter X is expressed as fraction of 10^n units (the units are cm, g, s). A useful characteristic of the disk is its maximum temperature, which occurs at $r = (49/36)R_{\text{acc}}$ and has a value $0.488 T_*$.

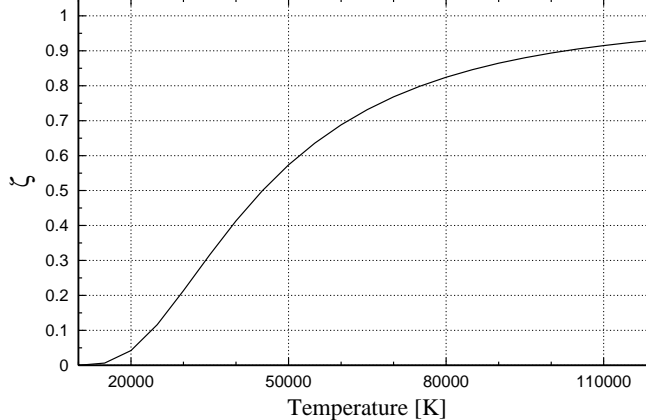


Fig. 2. Parameter ζ as a function of the blackbody temperature. It represents a fraction of the hot star luminosity below 912 Å (Sect. 4.2).

The final stage of the mass transferred throughout the accretion disk is its deceleration and landing onto the accreting star. This happens in the so called *boundary layer* (BL), in which the inner disk material loses its kinetic energy to match the surface velocity of the star. If the accreting star rotates at a small fraction of its breakup velocity, then the BL emits a luminosity comparable to that of the disk. Contrary, when the star rotates close to breakup, there should be little emission from the BL (e.g. Warner, 1995). The geometry of the BL can be approximated by a ring with thickness $2H$ surrounding the accreting star. Then the luminosity, L_{BL} , of its area, $2\pi R_{\text{acc}} 2H$, for a non-rotating star is comparable to that of the accretion disk. So,

$$L_{\text{BL}} = 4\pi R_{\text{acc}} H \sigma T_{\text{BL}}^4 \equiv \frac{1}{2} \frac{G M_{\text{acc}} \dot{M}_{\text{acc}}}{R_{\text{acc}}} = L_{\text{AD}}. \quad (5)$$

The effective temperature of the BL can be derived with the help of Eq. 5, and according to Warner (1995) it can be approximated as

$$T_{\text{BL}} \approx 2.9 \times 10^5 M_1^{1/3}(\text{acc}) R_9^{-7/9}(\text{acc}) \dot{M}_{18}^{2/9}(\text{acc}) \text{ K}. \quad (6)$$

In the following section we use these components of radiation to fit the observed SED.

4 Modeling the UV/optical continuum

4.1 The uneclipsed nebula

Figure 1 shows a faint component of the nebular radiation seen during eclipses. We compared a grid of models of the nebular continuum to these fluxes and

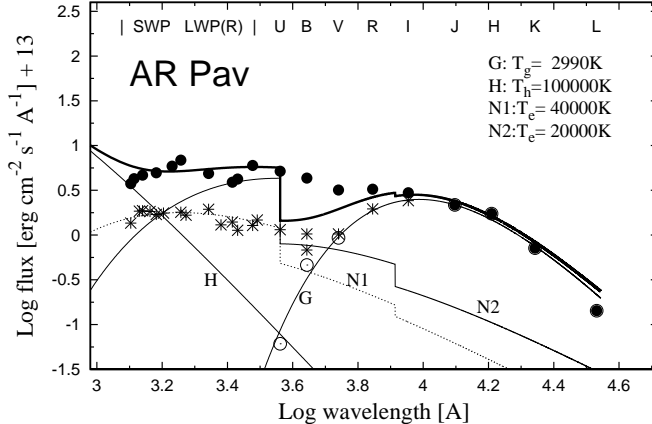


Fig. 3. Comparison of the observed AR Pav continuum and calculated according to an ionization model: Hot star ($T_h = 10^5$ K) ionizing the circumbinary medium giving rise to the nebular continuum ($T_e = 20\,000$ K). Solid thick line represents superposition of all components (G+H+N1+N2). These models are not able to give satisfactory agreement with observations (Sect. 4.2).

selected that with $T_e = 40\,000 \pm 5\,000$ K, which corresponds to the best fit to observations (Fig. 1). Luminosity of this nebular emission is $L_N \sim 500 (d/4.9 \text{ kpc})^2 L_\odot$. The uncertainty in T_e results from that in fluxes as given by the IUE observations (about 10%, in average). An analysis of the $\chi^2(T_e)$ function is described in Skopal (2001).

4.2 SED of an ionization model

During quiescent phases of symbiotic binaries the hot component ($T_h \approx 10^5$ K) ionizes a fraction of the neutral wind of the cool giant giving rise to the nebular continuum ($T_e \approx 1.5 - 2.0 \times 10^4$ K). As a result the UV/optical continuum is given by superposition of the stellar and nebular components of radiation. Below we test this possibility for the case of AR Pav.

The maximum luminosity of a blackbody hot star of a radius R_h and temperature T_h , which can be converted into the nebular radiation is

$$4\pi R_h^2 \int_0^{912} \pi B_\lambda(T_h) d\lambda = \zeta L_h \quad \text{erg s}^{-1}, \quad (7)$$

where the factor ζ (< 1) represents the fraction of the hot star luminosity, L_h , below 912 Å. It is a strong function of the blackbody temperature between 20 000 and 60 000 K (Fig. 2). Under assumption that the ionized medium is optically thick in the Lyman continuum, i.e. all the photons with $\lambda < 912$ Å are converted into the nebular emission, the maximum nebular luminosity can

be expressed as

$$L_{\text{neb}}^{\max} = \int_{912}^{\infty} \varepsilon_{\lambda} d\lambda \int_V n_+ n_e dV = \zeta L_h \text{ erg s}^{-1}. \quad (8)$$

Thus if the near-UV continuum is of the nebular nature, then for the observed flux, for example at $\lambda=3600 \text{ \AA}$, $F_{3600}^{\text{obs}} \sim 5 \times 10^{-13} \text{ erg cm}^{-2} \text{ s}^{-1} \text{ \AA}^{-1}$ (Table 1), the distance $d = 4.9 \text{ kpc}$ and the emission coefficient $\varepsilon_{3600} = 2.6 \times 10^{-28} \text{ erg cm}^3 \text{ s}^{-1} \text{ \AA}^{-1}$ ($T_e = 20000 \text{ K}$), we get by using Eq. 1 the emission measure $EM = \int_V n_+ n_e dV = 5.5 \times 10^{60} \text{ cm}^{-3}$ and according to Eq. 8

$$L_{\text{neb}}^{\max} = EM \int_{912}^{\infty} \varepsilon_{\lambda} d\lambda \dot{=} 1230 L_{\odot}. \quad (9)$$

The corresponding minimum of the hot star luminosity, which is capable of producing such nebular emission, is $L_h^{\min} = L_{\text{neb}}^{\max}/\zeta = 1380 L_{\odot}$ for $T_h = 10^5 \text{ K}$ ($\zeta = 0.89$). To compare the model with observations, first, we scaled the emission coefficient ε_{λ} to fluxes between $\lambda 3000\text{--}3600 \text{ \AA}$, where the nebular component of radiation dominates the SED in the ionization model. The scaling factor $k_N = F_{\lambda}^{\text{obs}}/\varepsilon_{\lambda} = EM/4\pi d^2$. Second, we scaled the hot star radiation with a factor $k_h \geq L_h^{\min}/4\pi d^2 \sigma T_h^4$ to match observations in the far-UV. Figure 3 shows our best solution, given by superposition of the nebular continuum with $T_e = 20000 \text{ K}$ and a hot stellar source ($L_h \sim 2.5 \times L_h^{\min}$, $T_h = 10^5 \text{ K}$), which roughly matches the observed UV continuum with a larger deviation at the far-UV. Cases with $T_e > 20000 \text{ K}$ significantly exceed the far-UV fluxes, and those with $T_e < 20000 \text{ K}$ cannot produce its rather flat profile. All cases do not match the optical continuum. Finally, the hot star with a lower temperature transforms a smaller fraction of its stellar radiation into the nebular (e.g. $T_h = 5 \times 10^4 \text{ K}$ gives $\zeta = 0.57$), which then requires too high L_h^{\min} other than to match the SED in the far-UV.

This analysis shows that the observed SED of the AR Pav UV continuum does not correspond to that of the ionization model of symbiotic binaries during quiescent phases. On the other hand, the presence of highly ionized emission lines in the UV spectrum (Hutchings et al., 1983) and the nebular emission during eclipses indicate a source of ionizing photons in the system.

4.3 SEDs with accretion disk

In accordance with previous suggestions, here we will fit the UV/optical/near-IR continuum of the hot object in AR Pav by models with an accretion disk as introduced in Sect. 3.2.

4.3.1 SED with a single accretion disk

Here we calculated a grid of models of fluxes given by Eq. 2 for fixed values of M_{acc} and \dot{M}_{acc} , but different R_{acc} , and selected that giving the best fit to the observed fluxes under conditions of the least square method.

According to Schild et al. (2001) we adopted the mass of the donor (the giant star) $M_g = 2 M_{\odot}$ and that of the accretor $M_{\text{acc}} = 0.75 M_{\odot}$. The rate of period change $\dot{P} = -3.5 \times 10^{-5}$ (Skopal et al., 2000a), the mass ratio $q = M_g/M_{\text{acc}} = 2.7$ and the orbital period of 605 days yield the accretion rate $\dot{M}_{\text{acc}} = 1.7 \times 10^{-5} M_{\odot} \text{ yr}^{-1}$ for the Roche lobe overflow if the transferred mass and its angular momentum are conserved in the system (Pringle and Wade, 1985, see Sect. 5.1 for more details). Using these values of M_{acc} and \dot{M}_{acc} to fit the component of radiation supposed to be due to the accretion disk (= SED - N - G; Fig. 4) by Eq. 2, we found the best solution for $R_{\text{acc}} = 0.78 R_{\odot}$ (Fig. 4, Table 2). We integrated the disk contributions to its outer radius $R_d = 10 R_{\odot}$, which can be considered as the smallest dimension of the disk for these parameters. This is because the disk temperature between the surface of the accretor and $r \sim 10 R_{\odot}$ is higher than 5 000 K, and thus radiative contributions of this part of the disk are important to explain the UV/optical SED (i.e. R_d cannot be smaller than $10 R_{\odot}$), but the disk annuli with $r > 10 R_{\odot}$ (i.e. $T(r) < 5000 \text{ K}$) do not contribute significant emission at UV/optical wavelengths, and are negligible with respect to the radiation of the giant in the IR region (i.e. R_d can be larger than $\sim 10 R_{\odot}$). Superposition of the considered components of radiation here (G, N, AD) matches well the observed SED of AR Pav (Fig. 4). This model expresses the round profile of the far-UV continuum, the flat near-UV/optical continuum and a relatively significant (with respect to the ionization model) contribution to the near-IR continuum of the giant. Note that we observe about 0.2 mag deep eclipse even in the I band (Menzies et al., 1982).

The accretion disk luminosity here, $L_{\text{AD}} \sim 1700 (d/4.9 \text{ kpc})^2 L_{\odot}$, can be balanced by the energy liberated in an accretion process for large accretion rates of $\dot{M}_{\text{acc}} > 10^{-4} M_{\odot} \text{ yr}^{-1}$ (Table 2). In addition, for the orbital inclination of $\approx 70^\circ$ (Sect. 5.2), and assuming the disk plane to be coplanar with it, the total disk luminosity is by a factor of about 1.5 larger ($L_{\text{AD}}^{\text{obs}} \approx 2 \cos(i) L_{\text{AD}}$). As discussed below (Sects. 5.1 and 5.2), observations do not contradict such a large \dot{M}_{acc} for a certain period of evolution of the giant star in AR Pav.

4.3.2 SED with the boundary layer and accretion disk

To calculate the flux contributions from the BL we assumed that this region can be approximated by a blackbody at a constant temperature T_{BL} (Eq. 6). In our procedure we fitted superposition of fluxes from the accretion disk and

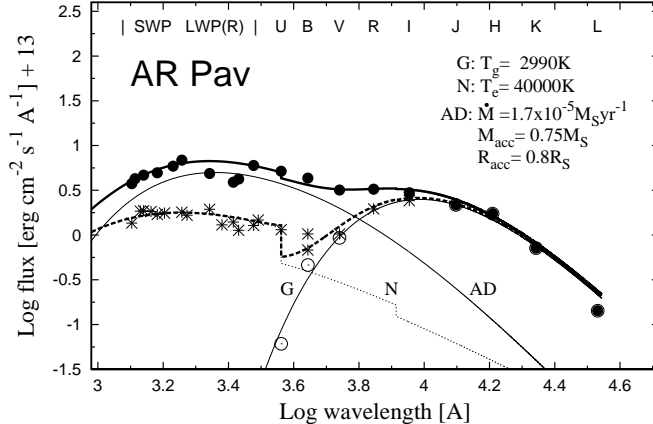


Fig. 4. Comparison of the AR Pav continuum and the calculated flux distribution for an accretion disk (AD). Solid thick line represents the resulting continuum given by the sum of all components of radiation (G+N+AD). Dashed thick line as in Fig. 1. This model is described in Sect. 4.3.1.

the BL,

$$F_\lambda = F_\lambda(AD) + \pi B_\lambda(T_{BL}), \quad (10)$$

to the observed SED, where $F_\lambda(AD)$ is given by Eq. 2. First, we scaled contributions from the BL with a factor

$$k_{BL} = \int_{\lambda} F_\lambda(AD) d\lambda / \sigma T_{BL}^4 \quad (11)$$

to satisfy conditions of Eq. 5. Second, we calculated a grid of models for $M_{acc} = 0.75$ and $1.0 M_\odot$, $R_d = 30 R_\odot$, \dot{M}_{acc} between $1.0 \cdot 10^{-5}$ and $5.0 \cdot 10^{-4} M_\odot yr^{-1}$ and R_{acc} between 0.1 and $3.4 R_\odot$. Finally, we selected models, for which the function

$$\chi^2(M_{acc}, \dot{M}_{acc}, R_{acc}) = \sum (F_\lambda^{\text{obs}} - F_\lambda(M_{acc}, \dot{M}_{acc}, R_{acc}))^2 / N \quad (12)$$

reached a minimum. We used fluxes from 1270 to 7000 Å (Table 1), but omitted those at 2200, 2600 and 2700 Å, i.e. $N = 11$. The function χ is plotted in Fig. 5. As can be seen from this figure there is no satisfactory solution. The best fits correspond to radii R_{acc} between 0.7 and $2.5 R_\odot$ and the BL temperature $T_{BL} \sim 40000 - 60000$ K. The impossibility to obtain a better solution is reflected by the too low required temperature of the BL, of which the flux dominates the far-UV wavelengths. Figure 6 shows an example. The results of this section suggest that the BL emission is not important to fit the AR Pav SED. Below, in Sect. 5.3, we discuss the BL emission in more detail.

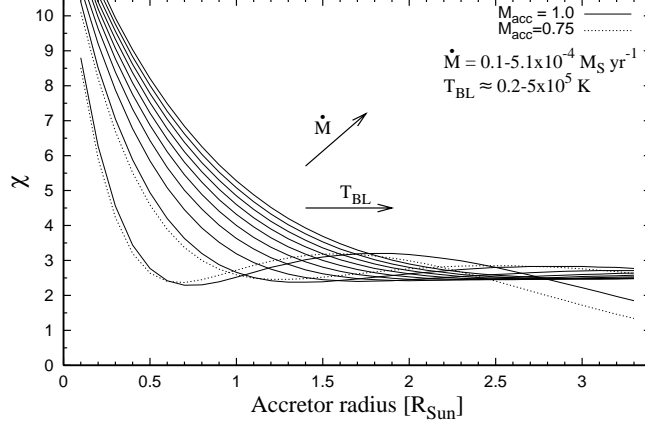


Fig. 5. The quantity χ as given by Eq. 12 in modeling the observed SED by the BL and accretion disk contributions. Solid lines represent models for $M_{\text{acc}} = 1 M_{\odot}$ and $\dot{M}_{\text{acc}} = 0.1 - 5.1 \times 10^{-4} M_{\odot} \text{ yr}^{-1}$. Compared are also two χ functions for $M_{\text{acc}} = 0.75 M_{\odot}$ (dotted lines). The minima of χ correspond to $T_{\text{BL}} \sim 40\,000 - 60\,000 \text{ K}$. Their large values reflect poor fits of these models to observations (Sect. 4.3.2, Fig. 6).

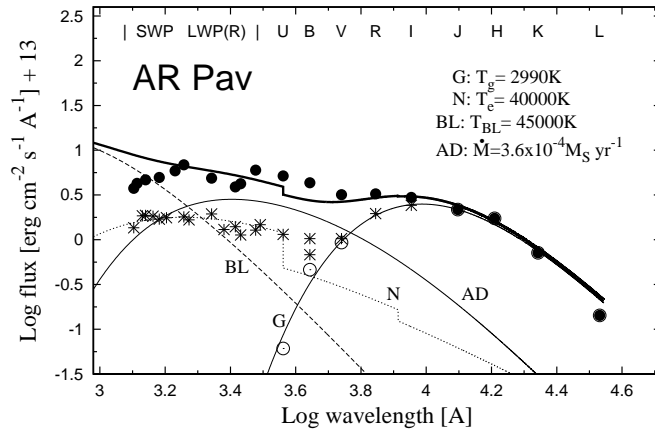


Fig. 6. One example from the best solutions of fitting the SED by the accretion disk and its BL flux contributions. The fits are very poor, because of a significant contribution of the BL in the far-UV wavelengths. This model is described in Sect. 4.3.2

5 Discussion

5.1 A mass transfer problem in AR Pav

The accretion rate of $1.7 \times 10^{-5} M_{\odot} \text{ yr}^{-1}$ (Sect. 4.3.1) derived from the orbital period change corresponds to the conservative mass transfer from the giant star onto its companion. However, successful fits of the UV continuum require at least one order of magnitude higher rates to balance the observed luminosity. This discrepancy can be caused by mass loss from the system, which makes the orbital period increase (cf. Soberman, Phinney and van den Heuvel, 1997).

Table 2
Examples of models of the SED for selected values of \dot{M}_{acc} .

R_{acc}	R_{d}	\dot{M}_{acc}	L_{acc}	$T_{\text{max}}/T_{\text{BL}}$	$\chi/10^{-13}$
$[R_{\odot}]$	$[R_{\odot}]$	$[M_{\odot} \text{ yr}^{-1}]$	$[L_{\odot}]$		[K]
Accretion disk (Sect. 4.3.1)					
3.7	40	$1.7 \cdot 10^{-3}$	5410	16600/46100	0.08
1.7	20	$1.7 \cdot 10^{-4}$	1180	16000/50600	0.09
0.78	10	$1.7 \cdot 10^{-5}$	257	16800/55600	0.11
0.01	0.1	$3.3 \cdot 10^{-11}$	0.04	16500/88500	0.07
Accretion disk and the boundary layer (Sect. 4.3.2)					
2.0	30	$2.1 \cdot 10^{-4}$	1240	15600/46700	2.51
2.5	30	$3.6 \cdot 10^{-4}$	1700	15100/44300	2.53

Notes: In all cases $M_{\text{acc}} \equiv 0.75 M_{\odot}$, $L_{\text{acc}} = 1/2 G M_{\text{acc}} \dot{M}_{\text{acc}} / R_{\text{acc}}$.

So, the mass transfer rate and the mass loss rate rival each other in the orbital period change. Mass loss from AR Pav is indicated by radial velocities of absorption components of hydrogen lines. Already Mayall (1937) revealed a P-Cygni type of hydrogen line profiles on three plates from 1900, 1901 and 1908. Thackeray and Hutchings (1974) measured absorption components of the H γ and/or H δ line profiles between 1953 and 1972. They determined an average position of these absorptions at -85.2 km s^{-1} . Recently, Quiroga et al. (2002) measured radial velocity of the central absorption component of H α at -96 km s^{-1} on spectra taken between 1988 and 2001. These values are shifted by -17 to -28 km s^{-1} relative to the systemic velocity (-68 km s^{-1} , Schild et al., 2001; Quiroga et al., 2002) and thus reflect a mass loss from the system. Under such conditions the observed decrease in the orbital period requires a much higher mass transfer than that given by conservative case. Therefore, the mass transfer rate (i.e. the accretion rate) of $1.7 \cdot 10^{-5} M_{\odot} \text{ yr}^{-1}$ can be considered only as a lower limit. This fact allow us to estimate the accretor radius $R_{\text{acc}} > 0.1 R_{\odot}$ for $M_{\text{acc}} = 0.75 - 1.0 M_{\odot}$ to balance the observed accretion luminosity irrespectively to the accretion disk model. Such the large R_{acc} precludes a white dwarf to be the accreting star in AR Pav.

5.2 Roche lobe overflow or a wind accretion?

Observations and the model energy distributions discussed in this paper suggest that the sole energy source in AR Pav is accretion. This view is also supported by the behaviour in its historical, 1889-2001, light curve, in which no large (5 - 7 mag) outbursts as in symbiotic novae have been observed (see

Skopal et al., 2001a). In addition, the light curve has characteristic features similar to those observed in CVs (Mayall, 1937; Skopal et al., 2000a), which suggests that the basic principles of mass transfer in AR Pav are similar to those of CVs. These arguments suggest that the red giant in AR Pav fills up (or is close to) its Roche lobe. Contrary, if the giant in AR Pav underfills its Roche lobe, then the mass transfer is via accretion from a stellar wind. However, this cannot be true. If this were the case, there would have been a huge (unrealistic) mass loss via the wind (at least of $10^{-3} M_{\odot} \text{ yr}^{-1}$) to get the accretion rate required to balance the observed luminosity of the hot object. In that case, the wind mass loss would make the orbital period *increase*, while the observations show that the period *decreases*. The latter can only be due to the Roche lobe overflow.

Other observational results allow this possibility. For example, the giant's radius inferred from eclipses, $R_g/A = 0.30 \pm 0.02$ (Skopal et al., 2000a), is equal to its volume-equivalent Roche radius for the orbital inclination of 70° (Quiroga et al., 2002). The V-shape of the eclipse profile supports this possibility (e.g. Fig. 8 of Skopal et al., 2000a). Further, the 106-day periodic variation with the amplitude of a few $\times 0.01$ mag observed in the visual light curve (Skopal et al., 2000a) could be understood as a response of the giant's radius to its mass loss. Generally, after losing an amount of mass, the giant will restore its hydrostatic equilibrium, which leads to variation in difference of the radius of the star and its Roche lobe. In the case of the presence of a deep convective envelope in the giant star, its radius rapidly increases and the star can run into a violent mass loss instability (see Soberman, Phinney and van den Heuvel, 1997; Shore, Livio and van den Heuvel, 1994, for more detail). Such a transient high mass transfer rate from the red giant to the hot component could be responsible for a higher level of the AR Pav activity observed during 1900-01, 1935-36 and 1985-99 (Skopal et al., 2000b).

5.3 Boundary layer emission in AR Pav

The nebular component of radiation indicates the presence of a hot ionizing source in AR Pav. In the models with accretion disk the ionizing source is represented by the BL.

The nebular emission has a luminosity $L_N \gtrsim 500 (d/4.9 \text{ kpc})^2 L_{\odot}$ (= uneclipsed nebula without emission lines), which places strong constraint on the BL luminosity and ionizing capacity. For parameters of the fit shown in Fig. 4 and described in Sect. 4.3.1, $L_{\text{BL}} (\equiv L_{\text{acc}}) \sim 1200 L_{\odot}$ and $T_{\text{BL}} \sim 51\,000 \text{ K}$ (Table 2). To balance the L_N luminosity, a fraction of the BL emission below 912 \AA has to be

$$L_{\text{BL}}(\lambda < 912 \text{ \AA}) = \zeta L_{\text{BL}} > 500 L_{\odot}. \quad (13)$$

For $L_{\text{BL}} = 1200 (d/4.9 \text{ kpc})^2 L_{\odot}$, Eq. 13 yields the factor $\zeta > 0.42$, which forces $T_{\text{BL}} > 40\,000 \text{ K}$ (Fig. 2). Thus the BL characterized by these quantities can balance well the observed nebular luminosity, L_{N} .

However, our modeling the SED *with* the BL (Sect. 4.3.2, Table 2) does not provide satisfactory fit (Figs. 5, 6). This implies that we cannot see the hotter inner parts of the disk and that any radiation generated in the BL is absorbed and diffused in the disk in the direction to the observer, but it is free in directions to the poles to ionize there the circumstellar matter. This situation thus produces two components of radiation of a very different temperature regimes observed in the ultraviolet spectrum: A relatively cool continuum, which was investigated in this paper, and a hot ionizing source seen through the nebular emission.

It is plausible that the lack of the BL emission in the continuum results only from a different real geometry of the accretion disk (probably more extended at its edge) than we adopted in our modeling (Eq. 2). So, if the disk is rather thick in its outer parts, then we can see essentially only its outer edge, which occults the BL at the disk's center for a high orbital inclination. Such a disk structure was suggested for the first time by Plavec and Hubeny (1994) for interacting binaries in which the accreting star is non-degenerate.

5.4 Configuration of the hot object and the eclipse profile

Our models of the observed SED (Sects. 4.1, 4.3.1) suggest that the hot object in AR Pav consists of an accretion disk around a central star embedded in a hot corona. This basic configuration can be independently verified by the eclipse profile, which is a function of wavelength. In the following two sections we therefore explore its two main characteristics – the different eclipse depth and width in the UV/optical/near-IR region on the basis of our model with accretion disk.

5.4.1 Depth of eclipses

Already Hutchings et al. (1983) noted that there is no total eclipse below 3600 \AA , and 70% of the hottest continuum (below 1400 \AA) is seen even at central eclipse. Recently Schild et al. (2001) demonstrated this behaviour on the ultraviolet IUE light curves.

Generally, the eclipse depth is given by the ratio of fluxes observed *in* and *out* of eclipse. In view of our models, it is determined by the ratio of the N+G to all considered components of radiation. In Fig. 7 we compared the modeled eclipse depth according to the solution shown in Fig. 4 and that observed in

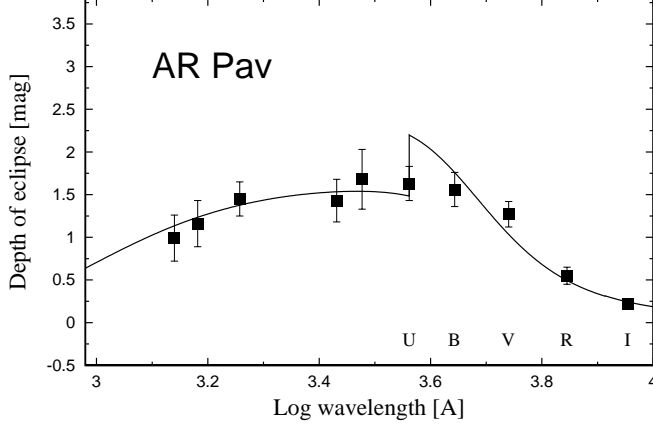


Fig. 7. Wavelength-dependent depth of eclipses measured in the dereddened UV/optical/near-IR light curves (full boxes). The solid line represents calculated eclipse depth according to our model in Fig. 4.

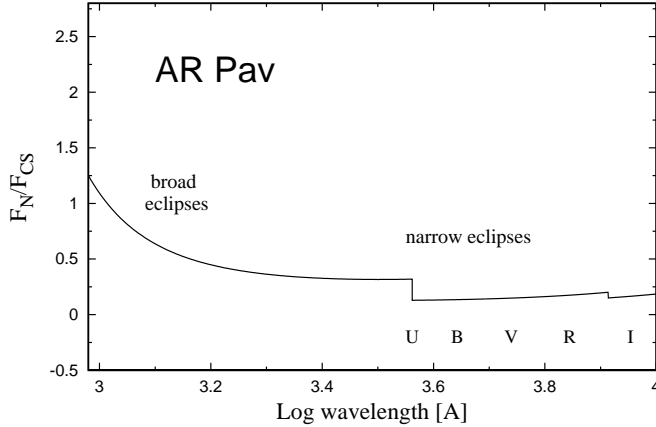


Fig. 8. The ratio of the hot object fluxes, F_N and F_{CS} , for the solution shown in Fig. 4. This characterizes the broadening of the eclipse profile (see text).

the light curves (cf. Schild et al., 2001; Andrews, 1974; Menzies et al., 1982). We can see that our model explains well the wavelength-dependent depth of eclipses.

5.4.2 Width of eclipses

Observations show a very broad eclipse profile in the far-UV ($\Delta\varphi \gtrsim 0.2\text{--}0.3$ of the orbital phase, Schild et al., 2001), while in the optical/near-IR the profile is characterized by a narrow core ($\Delta\varphi \lesssim 0.1$) with shallow wings (Andrews, 1974; Menzies et al., 1982). The hot object in AR Pav consists of basically two components – the extended nebula and the central star with an accretion disk. Let f_N and f_{CS} be the fluxes emitted by a surface element of the projected nebula and the central source, respectively, to the sky. The observed eclipse profile then can be characterized by the ratio f_N/f_{CS} . The case of $f_N/f_{CS} \approx 1$ makes the eclipse profile very broad, because the extended nebula contributes significant emission with respect to that of the small central source. On the

other hand, $f_N/f_{CS} \ll 1$ results in a narrow eclipse core determined by the central source, accompanied with shallow wings as the nebula is faint (see also Fig. 4 of Skopal et al., 2001b). In our approximation and for a spherical nebula, it is simple to find that

$$f_N/f_{CS} \propto F_N/F_{CS}, \quad (14)$$

where F_N and F_{CS} are integrated fluxes of the nebula and the central source at a given wavelength. Figure 4 shows that the ratio F_N/F_{CS} is a function of the wavelength, which thus represents the primary cause of the observed wavelength-dependent eclipse width. Therefore, we plotted this ratio in Fig. 8 according to modeled components of radiation shown in Fig. 4. In the effect of relation (14), Fig. 8 shows that

$$(f_N/f_{CS})_{uv} > (f_N/f_{CS})_{opt}, \quad (15)$$

which answers the question why the eclipses are broader in the ultraviolet than in the optical/near-IR region. A more rigorous approach, in which the parameter f_N/f_{CS} is treated as a function of the radial distance from the central object, would give a more accurate information about the nebula structure. However, this analysis is beyond the scope of this paper.

6 Conclusions

The results of this study may be summarized as follows:

- (i) Based on the ultraviolet IUE low-resolution spectra and the broad-band optical and infrared *UBVRI* and *JHKL* photometry, we re-constructed the SED in the AR Pav continuum between 0.12 and 3.4 μ m. By this way we revealed a very high luminosity of the hot object in the binary, $L_h \sim 2\,200 (d/4.9 \text{ kpc})^2 L_\odot$.
- (ii) We failed to fit the UV/optical continuum of the hot object by a standard ionization model of symbiotic binaries. This suggests that the configuration of AR Pav differs significantly from the typical configuration of symbiotic binaries during their quiescent phases.
- (iii) The UV/optical/IR SED can be fitted by a simple blackbody accretion disk embedded in an extended hot corona ($T_e = 40\,000 \pm 5\,000 \text{ K}$). The standard thin disk model requires a high accretion rate $\dot{M}_{\text{acc}} > 2 \times 10^{-4} M_\odot \text{ yr}^{-1}$ onto the central star with a radius $R_{\text{acc}} \gtrsim 2 R_\odot$. Any accretion process at $\dot{M}_{\text{acc}} > 1.7 \times 10^{-5} M_\odot \text{ yr}^{-1}$ (Sect. 5.1) for $M_{\text{acc}} = 0.75 - 1.0 M_\odot$ limits the accretor radius to $R_{\text{acc}} > 0.1 R_\odot$ to balance the observed accretion luminosity. This result suggests that the accreting star in AR Pav is non-degenerate.

- (iv) To basic configuration of the hot object – the accretion disk embedded in an extended nebula – allow us to understand the observed wavelength-dependent depth and width of the eclipse profile (Figs. 7, 8): The eclipse *width* results from that the hot object consists of the two geometrically very different components of radiation (N + AD), the ratio of which is a function of the wavelength. The eclipse *depth* is given by a different ratio of the uneclipsed (N+G) to the total light throughout the spectrum.
- (v) Models with the accretion disk and its BL ($L_{\text{BL}} \sim L_{\text{AD}}$) failed to fit the far-UV SED. However, the presence of a very hot region in the system is indirectly indicated through the strong nebular emission. This suggests that the hotter inner parts of the disk with the BL are permanently occulted by the disk material, when viewing the system (nearly) edge-on.

Acknowledgements

This research has been supported by the Slovak Academy of Science under a grant No. 1157. The author is grateful to Dr. D. Chochol for commenting on the manuscript, Dr. H.M. Schmid for his critical reading of an earlier draft of this paper, and an anonymous referee for several helpful comments.

References

Andrews, P.J., 1974, MNRAS, 167, 635.
 Bessell, M.S. 1983, PASP, 95, 480.
 Brown, R.L., Mathews, W.G., 1970, ApJ, 160, 939.
 Bruch, A., Niehues, M., Jones, A.F., 1994, AA, 287, 829.
 Glass, I.S., Webster B.L., 1973, MNRAS, 165, 77.
 Gurzadyan, G.A., 1997, *The Physics and Dynamics of Planetary Nebulae*, Springer-Verlag, Berlin.
 Hutchings, J.B., Cowley, A.P., Ake, T.B., Imhoff, C.L., 1983, ApJ, 275, 271.
 Kenyon, S.J., Webbink, R.F., 1984, ApJ, 279, 252.
 Léna, P., Lebrun, F., Mignard, F., 1999, *Observational Astrophysics*, Springer-Verlag, Berlin.
 Mathis, J.S., 1987, in: Y. Kondo (ed.), *Exploring the Universe with the IUE Satellite*, Reidel Publ. Comp., Dordrecht.
 Mayall, M.W., 1937, Harvard Annals, 105, 491.
 Menzies, J.W., Coulson, I.M., Caldwell, J.R.A., Corben, P.M., 1982, MNRAS, 200, 463.
 Plavec, M.J., Hubeny, I., 1994, in: A. Shafter (ed.), *Interacting Binary Stars*, A.S.P. Conf. Ser. Vol. 56, San Francisco, p. 87

Pringle, J.E., Wade, R.A., 1985, *Interacting Binary Stars*, Cambridge Univ. Press, Cambridge

Quiroga, C., Mikolajewska, J., Brandi, E., Ferrer, O., García L., 2002, AA, 387, 139.

Savage, B.D., Mathis, J.S., 1979, ARA&A, 17, 73.

Schild, H., Dumm, T., Mürset, U., Nussbaumer, H., Schmid, H.M., Schmutz, W., 2001, AA, 366, 972.

Shore, S.N., Livio, M., van den Heuvel, E.P.J., 1994, 'Interacting Binaries', Springer-Verlag, Heidelberg.

Soberman, G.E., Phinney, E.S., van den Heuvel, E.P.J., 1997, AA, 327, 620.

Skopal, A., 2001, Contr. Astron. Obs. Skalnaté Pleso, 31, 119.

Skopal, A., Djurašević, G., Jones, A., Drechsel, H., Rovithis-Livaniou, H., Rovithis, P., 2000a, MNRAS, 311, 225.

Skopal, A., Pribulla, T., Wolf, M., Shugarov, S., Jones, A., 2000b, Contr. Astron. Obs. Skalnaté Pleso, 30, 28.

Skopal, A., Kohoutek, L., Jones, A., Drechsel, H., 2001a, IBVS No. 5195.

Skopal, A., Teodorani, M., Errico, L., Vittone, A.A., Ikeda, Y., Tamura, S., 2001b, AA, 367, 199.

Thackeray, A.D., Hutchings, J.B., 1974, MNRAS, 167, 319.

Tylenda, R., 1981, Acta Astron., 31, 127.

Warner, B. 1995, *Cataclysmic Variable Stars*, Cambridge Univ. Press, New York.